Numerical Analysis on Shear Performance of Demountable Steel Ring Dowel Connections for Reusing Shear Walls

Zexiu Zhu[1], *Ray Kai Leung* Su[1*]

[1]Department of Civil Engineering, The University of Hong Kong, Pokfulam Road, Hong Kong

Abstract. Rapid development of the building industry significantly increases construction and demolition waste (CDW) and greenhouse gas emissions. Demountable structures can reduce CDW and increase construction efficiency by reusing prefabricated structural elements. Conventional structures are non-reusable since the connections between structural elements are irreversible wet joints. This study proposes a demountable steel ring dowel (SRD) connection for transferring shear between shear wall panels. In this study, a finite element model is established using software ABAQUS and validated with experiment results. The effects of shape, material strength, and tube thickness on the shear strength of the steel ring dowel connection are investigated through numerical simulation. The results show that hexagon-shaped SRD connections have a higher initial stiffness than square- or round-shaped SRD connections. Hexagon-shaped SRD connections have much higher shear bearing capacity than round-shaped SRD connections. The shear bearing capacity of SRD connections increases with increasing tube thickness and the material strength. As the tube thickness rises from 3 mm to 10 mm, the initial stiffness of SRD connections first increases drastically and then remains almost constant. Infilled concrete increases the shear strength of SRD connections. However, the load-displacement curves of SRD connections with infilled concrete under shear first drop after reaching peak load due to the concrete detachment and cracking, and then remain almost constant.

1 Introduction

In the current world, the building industry takes responsibility for a large quantity of carbon dioxide emissions [1]. One solution to mitigate this situation of environmental degradation is reusing buildings through demountable structural elements. However, most buildings cannot be reused since the structural elements (i.e., beams, columns, walls, and slabs) are joined with irreversible connections to guarantee structural integrity.

Dowel connections are generally applied in real-world practice to transfer shear force. Conventional concrete dowel connections are formed by pouring concrete into polygonal

* Corresponding author: klsu@hku.hk

gaps preserved in advance between structural components [2]. However, concrete is difficult to remove, and the strong bond effect between concrete dowel connections and structural components may cause damage during demolition. Recent studies on demountable shear wall connections focus on steel plate-bolt connections (SPBC). However, according to these studies, demountable shear walls fail at bolt holes due to local force concentration and exhibit slip between wall panels under horizontal forces [3, 4]. In 2020, Qing applied cast-in-place dowel connections in shear walls [5]. Results show that dowel connections can resist shear slip and provide high shear strength. However, these dowel connections are hard to disassemble and reuse.

This paper proposes an innovative steel ring dowel (SRD) connection to transfer shear force. The SRD connection is a dry connection and can address the safety concerns related to structural element disassembly. The objective of this paper is to investigate the influence of different parameters on the shear behaviour of SRD connections. In this study, finite element models of SRD connections are created for numerical analysis using the software ABAQUS. The influence of material strength, connection shape, and connection size is investigated.

2 Proposed SRD connection

The SRD connections are hollow polygonal steel tubes. SRD connections have the same shape as dowel connections, but do not bond wall panels and can therefore be disassembled. Fig. 1 presents the assembly sequence of the demountable shear wall with SRD connections. Shear walls can be easily disassembled and reused without damage by reversing the installation sequence. Steel plates provide moment resistance for shear walls under lateral loads. SRD connections can resist shear slip between wall panels to promote structural integrity and distribute forces concentrated at bolt holes, thereby increasing the strength of steel plate-bolt connections.

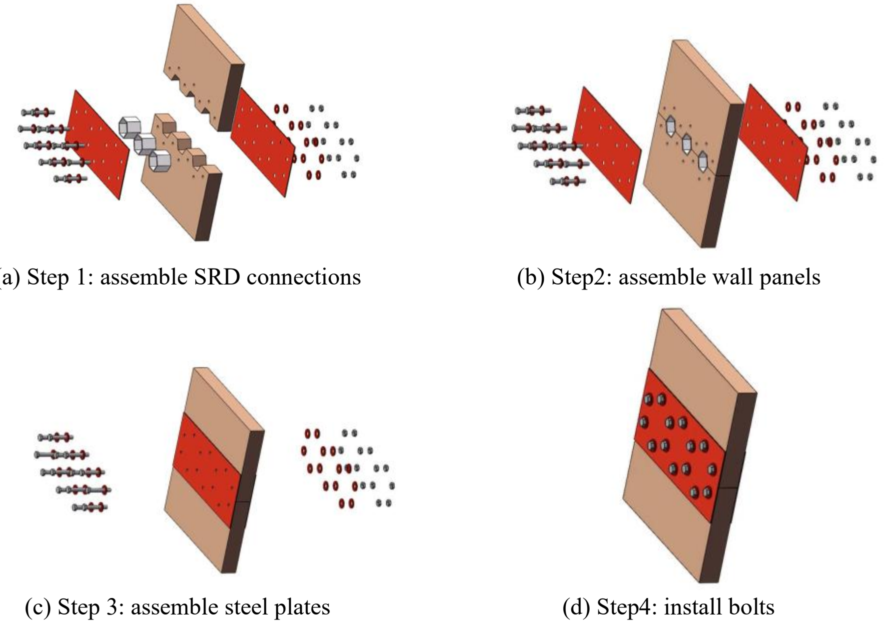

(a) Step 1: assemble SRD connections (b) Step2: assemble wall panels

(c) Step 3: assemble steel plates (d) Step4: install bolts

Fig. 1. Assembly sequence of the demountable shear wall.

3 Numerical analysis

3.1 Finite element models

3.1.1 Element details, meshing, interaction modeling, contacts, and boundary conditions

The finite element models were established following the guidance and recommendations provided by Tao Zhong and Dongxu Li through the software ABAQUS [6, 7]. C3D8R elements were used to model the steel tubes, steel plates, concrete, and loading modules. The mesh size of the steel tubes, steel plates, concrete, and loading modules were selected as $D_{\mathrm{st}}/25$, $L_{\mathrm{sp}}/25$, $D_{\mathrm{c}}/25$, and $L_{\mathrm{w}}/25$, where D_{st}, L_{sp}, D_{c} and L_{w} are the diameter of the steel tubes, length of the steel plates, diameter of concrete, and length of loading modules, respectively. "Hard contact" was defined in the normal direction for all contact surfaces. The Coulomb friction model was utilized to simulate the tangent contact. In this study, friction coefficients of 0.3 and 0.6 were employed for steel-to-steel and steel-to-concrete contact surfaces, respectively [7].

Fig. 2 illustrates the finite element model of the SRD connection with a regular hexagon shape. The established finite element model comprises three components. A 30 mm displacement is applied to the top surface of the loading module to investigate the shear performance of SRD connections.

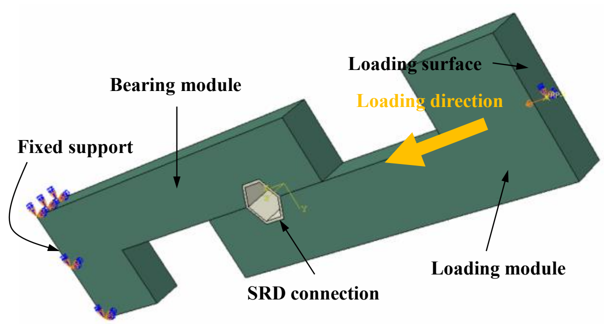

Fig. 2. Finite element model of SRD connections.

3.1.2 Material models

In this paper, Tao Zhong's three-stage model was selected to describe the behavior the infilled concrete, and a bilinear stress-strain model was applied to define the stress-strain relationship for all steel materials, as shown in Fig. 3. Concrete Damage Plasticity (CDP) model was used to define the concrete constitutive behaviour. The elastic modulus of concrete (E_{c}) was calculated by the empirical Equation $E_{\mathrm{c}} = 4733\sqrt{f_{\mathrm{c}}'}$ recommended in ACI 318-19 section 12.2.2.1, where f_{c}' is the concrete cylinder compressive strength [8]. The flow potential eccentricity (e) and viscosity parameters were adopted as 0.1 and 0, respectively. The ratio of initial equibiaxial compressive yield stress to initial uniaxial compressive yield stress can be determined based on Equation $f_{\mathrm{b0}}/f_{\mathrm{c}}' = 1.5(f_{\mathrm{c}}')^{-0.075}$ [9]. The following equation was adopted to calculate the parameter K for defining plasticity:

$$K = \frac{5.5}{5+2(f_{\mathrm{c}}')^{0.075}} \tag{1}$$

The dilation angle was taken as 40°. The following equation was utilized to describe the initial ascending curve OA [10]:

$$\frac{\sigma}{f_{\mathrm{c}}'} = \frac{A\cdot X + B\cdot X^2}{1+(A-2)X+(B+1)X^2} \tag{2}$$

Where $X = \frac{\varepsilon}{\varepsilon_0}$; $A = E_c \frac{\varepsilon_{c0}}{f_c'}$; $B = \frac{(A-1)^2}{0.55} - 1$. The strain at point A was taken as $0.00076 + \sqrt{(0.626 f_c'/f^* - 4.33) \times 10^{-7}}$, where f^* is equal to 1 MPa and f_c' is expressed in MPa [11]. The strain at point B can be taken as $\frac{\varepsilon_{cc}}{\varepsilon_{c0}} = e^k$. The parameter k can be calculated by the following equation:

$$k = (2.9244 - 0.00367 f_c') \left(\frac{f_B}{f_c'}\right)^{0.3124+0.002 f_c'} \tag{3}$$

Equation (4) was adopted to calculate the parameter f_B:

$$f_B = \frac{0.25 \cdot (1 + 0.027 f_y) \cdot e^{-0.02\sqrt{2D^2}/t}}{1 + 1.6e^{-10} \cdot (f_c')^{4.8}} \tag{4}$$

The descending curve BC was defined by the following equation:

$$\sigma = f_c' \left[0.1 + 0.9e^{-\left(\frac{\varepsilon - \varepsilon_{cc}}{\alpha}\right)^{0.92}}\right] \tag{5}$$

Where $\alpha = 0.005 + 0.0075 \frac{A_s f_y}{A_c f_c'}$; A_s and A_c are the areas of the cross-section of the steel tube and concrete, respectively. Elastic modulus and Poisson's ratio for structural steel were taken as 200,000 N/mm2 and 0.3, respectively. Poisson's ratio for infilled concrete was taken as 0.2.

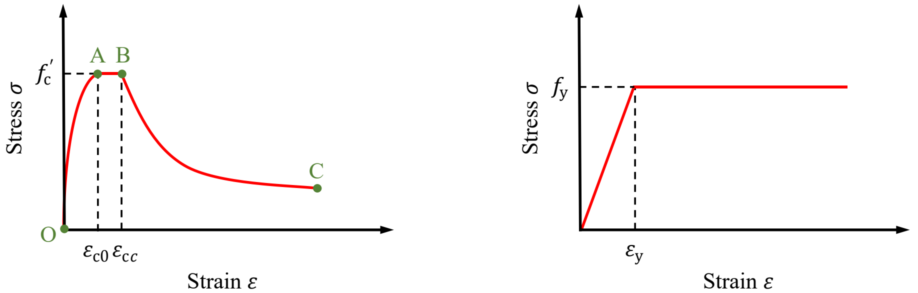

(a) Confined concrete (b) Structural steel

Fig. 3. Material constitutive models for structural steel and confined concrete.

3.2 Verification of the constructed numerical models

In this study, experiments conducted by Tomii and Schneider and test results were used to validate the reliability of the finite element model [12, 13]. Fig. 4 illustrates the comparisons of load-axial deformation curves between the test results and the analysis results from the numerical model.

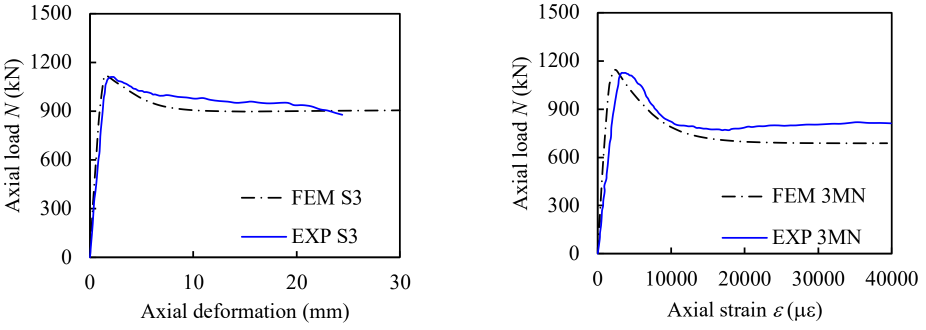

(a) Specimen S3 (b) Specimen 3MN

Fig. 4. Validation of the numerical model with test results.

3.3 Parameters to be investigated

Table 1 summarizes the values of the parameters to be investigated in this study. The first, second, and third groups investigate the effects of shape, thickness, and material strength, respectively, on the shear behaviour of SRD connections. Group III also investigates the effects of concrete on the shear behaviour of SRD connections. The diameter of the SRD connections is fixed at 150 mm. Only two SRD connections in group III have concrete filled inside.

Table 1. Values of parameters for numerical analysis.

Group	Shape	Diameter D	Thickness t	Yield strength f_y	Concrete strength f_c'
I	Round	150 mm	5 mm	235 MPa	Not applicable
	Square	150 mm	5 mm	235 MPa	Not applicable
	Hexagon	150 mm	5 mm	235 MPa	Not applicable
II	Hexagon	150 mm	3 mm	235 MPa	Not applicable
	Hexagon	150 mm	10 mm	235 MPa	Not applicable
III	Hexagon	150 mm	10 mm	355 MPa	Not applicable
	Hexagon	150 mm	10 mm	235 MPa	30 MPa
	Hexagon	150 mm	10 mm	235 MPa	45 MPa

3.4 Influence of shape on the shear performance of SRD connections

Fig. 5 shows the deformation of SRD connections with different shapes in group I. As shown in Fig. 5, the round-shaped and square-shaped steel rings exhibit significant uneven localized bending deformation under shear force, while the bending deformation of the hexagon-shaped steel ring focuses on the vertex of the hexagon.

Fig. 6 presents the load-displacement relationship of SRD connections. The results show that the initial stiffness of the hexagon-shaped SRD connection is larger than the round-shaped and square-shaped SRD connections. The shear resistance capacity of the hexagon-shaped and square-shaped SRD connections is much higher than the round-shaped steel ring. The shear resistance capacity of the square-shaped steel ring is slightly higher than the hexagon-shaped steel ring. The difference in stiffness and strength is because steel tubes bend at corners under shear stress, and the uniform distribution of corners in hexagonal and square steel tubes enables a greater portion of the tube wall to engage in resisting shear forces.

https://doi.org/10.1051/e3sconf/202672505002

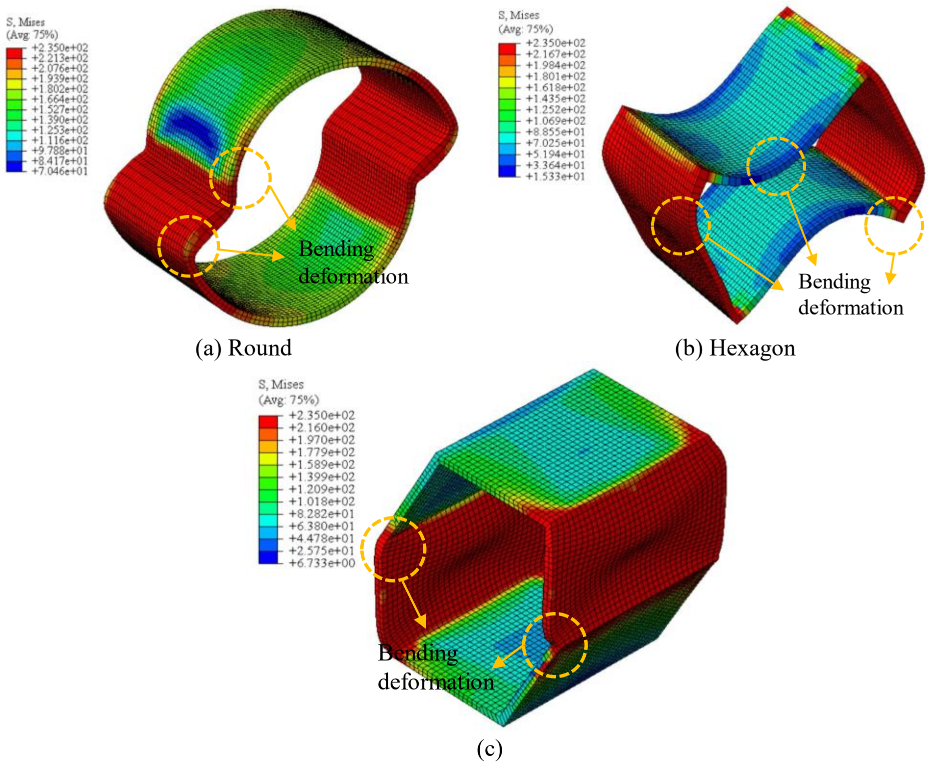

Fig. 5. Deformation of SRD connections in group I (scale factor = 1).

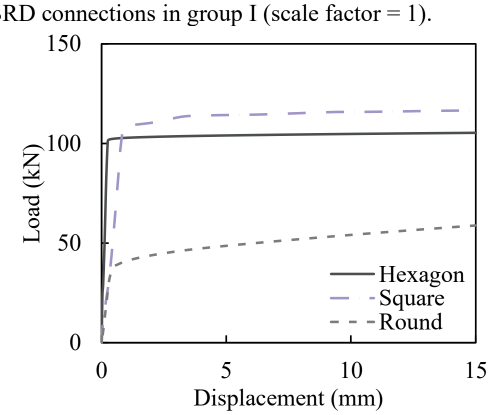

Fig. 6. Load-displacement relationship of SRD connections with different shapes.

3.5 Influence of size and material strength on the shear performance of SRD connections

Fig. 7(a) summarizes the load-displacement relationship of the hexagon-shaped SRD connections with different tube thicknesses. The results show that the hexagon-shaped SRD connection with a 3 mm-thick steel tube has lower initial stiffness than other SRD connections. With increased steel grade, the shear bearing capacity of the SRD connection increases. Fig. 7(b) summarizes the load-displacement relationship of the hexagon-shaped SRD connections with different material strength. The infilled concrete can significantly increase the shear strength of SRD connections. The shear bearing capacity of the SRD connection increases with increasing concrete strength. A drop in the load-displacement relationship of the hexagon-shaped SRD connections with infilled concrete can be observed after the curves reach peak load. This is because the concrete detaches from the steel tube wall and cracks.

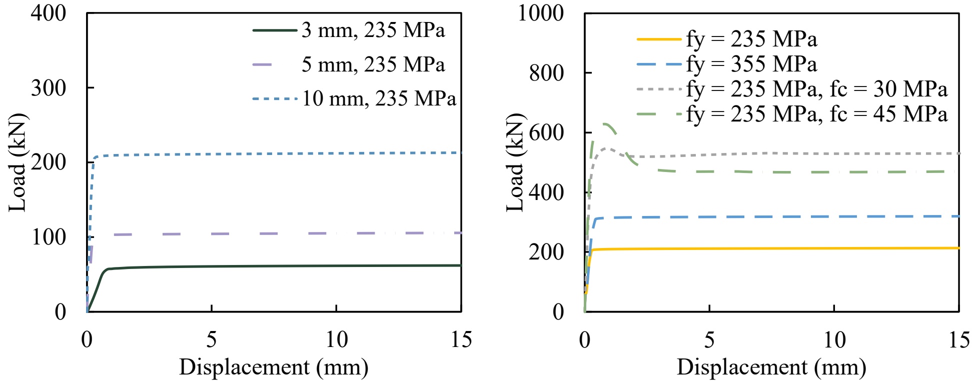

(a) Group II (b) Group III

Fig. 7. Load-displacement relationship of SRD connections with different material strength and steel ring thickness.

4 Conclusion

This study investigates the influence of shape, tube thickness, and material strength on the shear bearing capacity of SRD connections. The conclusions and design recommendations for SRD connections are summarized as follows:

1. The hexagon-shaped SRD connections have a larger initial stiffness than the square-shaped and round-shaped SRD connections due to a more even distribution of corner points. Hexagon-shaped and square-shaped SRD connections have much larger shear bearing capacity than round-shaped SRD connections. Hexagons are a more appropriate choice for SRD connection shapes than squares or circles.
2. The shear bearing capacity of SRD connections increases with increasing tube thickness. If the steel tube wall of hexagon-shaped SRD connections is excessively thin, the connection's initial shear stiffness is greatly reduced. As a result, the steel tube of SRD connections must have a thickness of at least 5 mm.
3. With increased material strength, the shear strength of the SRD connections increases. The infilled concrete can significantly increase the shear strength of SRD connections. The shear strength of SRD connections with infilled concrete decreases after the peak load due to concrete detachment and cracking. Inserting reinforcement may resist internal tension and prevent concrete detachment and cracking, thereby increasing the shear strength of SRD connections under large deformation.

This research is supported by a grant from the Research Grants Council of the Hong Kong Special Administrative Region, China (RGC Ref No. PolyU R5031-22F).

References

1. L. Chen, X. Ji, Z. Zhu, R.W.H. Wong, R.K.L Su, Structural Concrete : Journal of the FIB, **26**, 4 (2025)
2. M.A. Issa, H.A. Abdalla, Journal of Bridge Engineering, **12**, 3 (2007)
3. Y.C. Zhong, F. Xiong, M.M. Ran, J. Chen, Q. Ge, Y. Lu, Journal of Building Engineering, **52**, 104451 (2022)

4. H. Jiang, H. Qiu, J. Sun, E. del Rey Castillo, J.M. Ingham, Engineering Structures, **210**, 110293 (2020)
5. Q. Zhi, X. Xiong, W. Yang, S. Liu, J. Xiong, Materials, **13**, 7 (2020)
6. T. Zhong, Z.B. Wang, Q. Yu, Journal of Constructional Steel Research, **89**, 121 (2013)
7. D. Li, B. Uy, V. Patel, F. Aslani, Journal of Constructional Steel Research, **141**, 161 (2018)
8. ACI, Building Code Requirements for Structural Concrete (ACI 318-19): An ACI Standard (2019)
9. V.K. Papanikolaou, A.J. Kappos, International journal of solids and structures, **44**, 21 (2007)
10. A.K. Samani, M.M. Attard, Engineering Structures, **41**, 335 (2012)
11. D. Nicolo, B.L. Pani, E. Pozzo, Materials and Structures, **27**, 4 (1994)
12. M. Tomii, K. Yoshimura, Y. Morishita, Experimental studies on concrete filled steel tubular stub columns under concentric loading (1977)
13. S.P. Schneider, Journal of Structural Engineering, **124**, 10 (1998)